IEEE Photonics Journal
An IEEE Photonics Society Publication

Open Access

Broadband Polarization Splitter-Rotator and the Application in WDM Receiver

Volume 11, Number 1, February 2019

Yingxuan Zhao
Chao Qiu
Aimin Wu
Haiyang Huang
Jun Li
Zhen Sheng
Wei Li
Xi Wang
Fuwan Gan

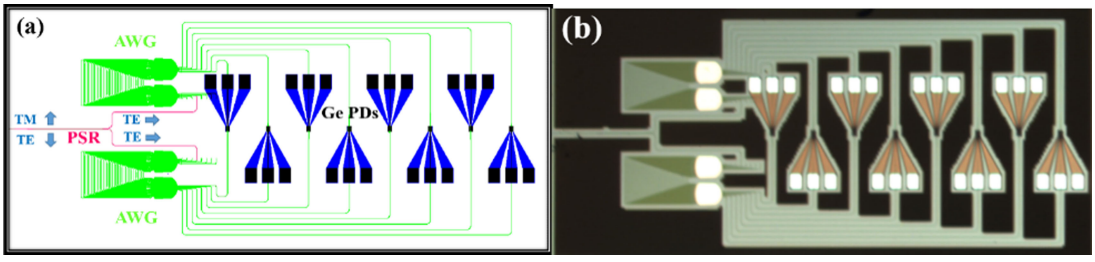

DOI: 10.1109/JPHOT.2018.2886268
1943-0655 © 2018 IEEE

IEEE photonics SOCIETY

IEEE

Broadband Polarization Splitter-Rotator and the Application in WDM Receiver

Yingxuan Zhao,[1,2] **Chao Qiu**,[1] **Aimin Wu**,[1] **Haiyang Huang**,[1] **Jun Li**,[1] **Zhen Sheng**,[1] **Wei Li**,[1] **Xi Wang**,[1] **and Fuwan Gan**[1,2]

[1]State Key Laboratory of Functional Materials for Informatics, Shanghai Institute of Microsystem and Information Technology, Chinese Academy of Sciences, Shanghai 200050, China
[2]University of Chinese Academy of Sciences, Beijing 100049, China

DOI:10.1109/JPHOT.2018.2886268

Manuscript received July 30, 2018; revised November 30, 2018; accepted December 8, 2018. Date of publication December 11, 2018; date of current version January 1, 2019. This work was supported in part by the National Key Research and Development Program of China under Grant 2017YFA0206403, in part by the National Natural Science Foundation of China under Grant 61475180, in part by the Science and Technology Commission of Shanghai Municipality under Grant 16ZR1442600, in part by the Strategic Priority Research Program of Chinese Academy of Sciences under Grant XDB24010400, and in part by the Shanghai Sailing Program under Grant 18YF1428100. Corresponding authors: Chao Qiu; Aimin Wu; Fuwan Gan (e-mail: cqiu@mail.sim.ac.cn; wuaimin@mail.sim.ac.cn; fuwan@mail.sim.ac.cn).

Abstract: Polarization sensitivity is a severe problem in photonic integration devices and chips based on the high-index contrast Si/SiO_2 system. In this paper, a broadband silicon polarization splitter-rotator (PSR) comprised of a bi-level taper and a counter-tapered coupler is proposed with a large fabrication tolerance. The measured insertion loss is lower than 0.7 dB/0.73 dB for the wavelength range from 1470 to 1580 nm with a crosstalk lower than −12.1 dB/−14.7 dB for TE and TM polarization input, respectively. By integrating the PSR with silicon arrayed waveguide gratings and germanium photodetectors (PDs) on a single chip, a polarization-insensitive wavelength-division-multiplexing (WDM) receiver is demonstrated with a polarization-dependent loss as low as 1.21 dB. High-speed operations are also achieved with clear eyes at 10 Gb/s.

Index Terms: Polarization splitter-rotator, silicon photonics, integrated photonic chips.

1. Introduction

In the past decades, silicon photonics technologies are greatly put forward for its small devices footprint, complementary metal oxide semiconductor (CMOS) process compatibility, and high integration level [1], [2], motived by the increasing demand from optical communications and interconnections [3]. WDM is an important solution to expand the data transmission capacity for both on-chip and off-chip optical networks [4], among which WDM receiver are one of the most critical component [5]. In a WDM receiver, optical signals carried by different wavelengths are transmitted in the same fiber or waveguide, and then demultiplexed and converted to electrical domain for subsequent processing.

One of the main challenges in the WDM receivers arises from polarization sensitivity. The large refractive index contrast between Si and SiO_2 results in strong polarization dependencies for silicon photonics devices based on nano-scale waveguides [6]–[8]. A polarization-diversity scheme has been proposed to address this issue [9], that is, the input light with arbitrary polarizations is first

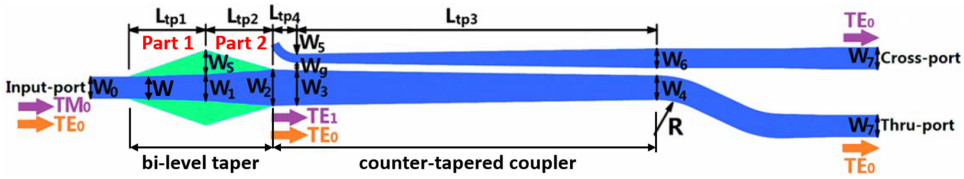

Fig. 1. Schematic of the proposed PSR comprised of a bi-level taper and a counter-tapered coupler. For the TM_0 mode input to the device, the bi-level taper works as a TM_0-TE_1 mode converter. Then through the counter-tapered coupler, the TE_1 mode is separated from the TE_0/TE_1 hybrid mode and convert to TE_0 mode. For the TE_0 mode input to the device, it remains unchanged in both bi-level taper and counter-tapered coupler.

split into two orthogonal components, and then one polarization state is rotated 90 degrees while the other component remains unchanged. The key components in this solution are the PSRs to split and rotate the beam polarization [10]. Tremendous efforts have been made in this field, and the mechanism of PSRs can be concluded into two groups based on mode coupling and mode hybridization respectively. Phase matching principle is used in mode-coupling designs such as bent directional coupler [11], [12] and taper-etched directional coupler [13], [14], which makes the type of devices extremely compact but wavelength and fabrication sensitive. On the contrary, devices based on mode hybridization usually have advantages in fabrication tolerances and insertion loss. The difference between the two groups lies in that the input TM polarization is first transferred to high order modes such as TE_1 before converted to TE_0. For instance, a PSR made on Si_3N_4 is demonstrated in Ref. [15], which has a bandwidth about 80 nm. In Ref. [16], a PSR based on bi-layer taper and Y junction with 50 nm bandwidth is proposed. In Ref. [17], a tapered waveguide followed by a 2×2 multimode interferometer was demonstrated with a wider operation bandwidth ($\sim$100 nm). These works are all based on mode hybridization principle, which have low loss and low crosstalk properties, while the operating bandwidth can be further improved to meet the requirement of practical applications.

In this work, a broadband silicon PSR comprised of a bi-level taper [18] and a counter-tapered coupler [19] is demonstrated. The bi-lever taper is designed with an asymmetric cross section, acting as a TM_0 -TE_1 mode converter. To separate the TE_1 and TE_0 modes, a counter-tapered coupler is used for its large bandwidth and fabrication tolerance. The device is completely compatible with CMOS platform. Benefitting from the asymmetric cross-section of the rib waveguide, SiO_2 cladding is used without the needs of silicon nitride or air cladding, facilitating large scale integrations with other photonic devices and even electronics parts. By integrating the silicon PSR with two 1×8 silicon AWGs and eight germanium photodetectors (PDs), the 8-channel WDM receiver is further demonstrated with PDL as low as 1.21 dB, achieving crosstalk below -15 dB.

2. Operation Principle and Simulation Results

The schematic structure of the PSR is shown in Fig. 1. The device is composed of an adiabatic bi-level taper and a counter-tapered coupler [20]. The blue regions represent fully-etched Si waveguides, and the green regions represent the partially etched slab waveguides. The thickness of the top silicon layer is 220 nm, and the slab height H_{slab} is 90 nm.

As can be seen in Fig. 1, to clearly interpret the working principle of the device, we intentionally divide the bi-level taper into two parts. The width of the Si waveguide is continuously increased from W_0 to W_1 in Part 1. There is a hybrid mode region for TM_0 and TE_1, where the principal and secondary components of the electric field of the hybrid modes are comparable. Ridge structures are employed to break the vertical symmetry of the waveguide. Therefore, the mode conversion of TM_0-TE_1 occurs during the light propagate from the input to the part 1 region. Part 2 of the bi-level taper is to adiabatically transmit the light wave from the double-layered waveguide to the slab waveguide. In this part, the width W_2 is carefully chosen to ensure low-loss transmission as well as to prevent the TE_1 mode returning to the TM_0 mode.

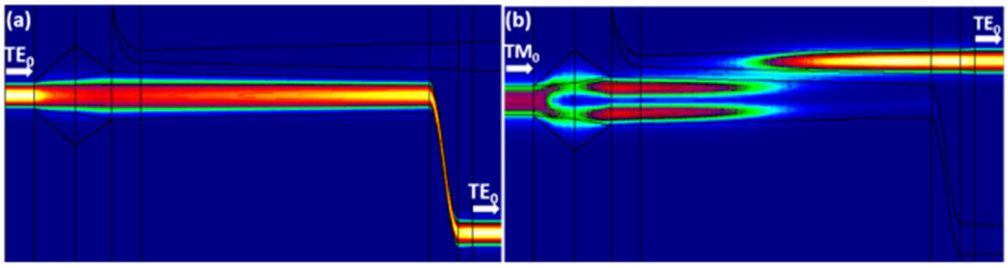

Fig. 2. Simulated electric field distributions at 1550 nm in the PSR for the (a) TE-and (b) TM-polarized inputs respectively. The fundamental TE mode passes through the device directly and exit from the lower port. While the fundamental TM mode convert to TE_1 mode first, after that the TE_1 mode couple to the cross port and convert into TE_0 mode.

TABLE 1
Parameters of PSR

Parameters of PSR (unit:μm)				
W_0	W_1	W_2	W_3	W_4
0.45	0.55	0.75	0.72	0.5
W_5	W_6	W_7	W_s	W_g
0.18	0.4	0.45	0.5	0.2
L_{tp1}	L_{tp2}	L_{tp3}	L_{tp4}	R
28.5	25	250	10	20

A directional coupler is connected to the bi-level taper for TE_1-TE_0 mode conversion. Directional coupler is widely used for its compact size and simple structure, however, strict phase matching is required, leading to a narrow bandwidth and stringent fabrication accuracy. In order to broaden the bandwidth and improve the fabrication tolerance, a counter-tapered structure is used in our design as shown in Fig. 1, whose two same slab waveguides are substituted by two parallel waveguides that gradually changed in the width. There exist a cross point that the effective refractive index of the TE_1 mode in the upper waveguide equals that of the TE_0 mode in the waveguide below. According to the mode evolution principle [20], mode coupling will occur so long as the two-waveguides system is long enough. Thus, even a small range of wavelength or width and thickness of the fabricated device changes, the effective refractive index cross points will shift, but mode coupling still occurs within the counter-tapered coupler. The overall performance will not be affected, indicating a large fabrication tolerance and broadband properties. A more detailed information of counter-tapered coupler can be referred to [21].

An arc waveguide is deliberately designed at the start section of the cross waveguide, connecting the bi-level taper and the counter-tapered coupler with the length L_{tp4}, which is utilized to reduce the coupling loss and radiation loss introduced by the discontinuity of the waveguide. At the end, an S-type waveguide is used between the counter coupler and the thru-port to reduce the crosstalk. Fig. 2 shows the simulated electric field distributions for TE_0 and TM_0 modes excited in the PSR. It can be clearly seen that the TE_0 mode passes through the device directly and exit from the through port, while the TM_0 mode will be converted to the TE_1 mode by the bi-level taper and then coupled to TE_0 mode in the cross port. All the parameters of device are shown in Table 1.

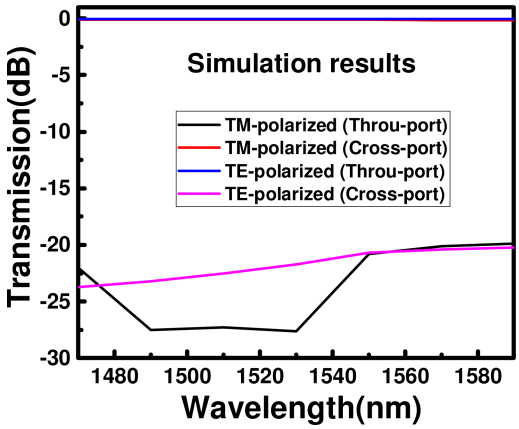

Fig. 3. Simulation results of the PSR. The simulated results shows the insertion loss is about 0.2 dB, and crosstalk is lower than −19 dB in the waveband from 1470 nm–1590 nm.

3. Measurement and Results

The proposed PSR was fabricated on a 0.13 μm CMOS platform. A silicon nitride (SiN) film is first deposited on the wafer surface using low-pressure chemical vapor deposition (LPCVD), which acts as a hard mask layer for the subsequent Si etching. 248 nm lithography is used to define the waveguide pattern. Silicon waveguides are formed using inductively coupled plasma reactive ion etching (ICP-RIE). To protect the waveguides from particles and damages, a thick silicon dioxide layer is deposited on the wafer surface finally. The measurement setup is shown in Fig. 4.

In the testing system, a tunable laser range from 1470 nm to 1580 nm is used. The input polarization state is set by a polarization splitting prism with a polarization controller. A straight waveguide is used as a control sample to align the output polarization plane with the input. The output polarization state is set by tuning the linear polarizer system in the dashed box. When the power-meter reaches its maximum value during the tuning, the output polarization state is regarded as the same with the input beam. The linear polarizer system consists of two fiber collimation devices and a NIR Polarizer. For the fabricated chip samples, the polarization components of the output light are selected by rotating the polarizer correspondingly [22].

The testing results of the fabricated PSR is shown in Fig. 5(a) and (b). The output is measured at the thru and cross ports with TE and TM polarization respectively. The overall loss of a reference straight waveguide is about −17 dB, including the coupling losses at both ends, linear polarizer system loss, and the total connection loss in the external system. The coupling loss can be further reduced by optimization of the edge couplers. As shown in Fig. 5, the TM polarization output at both ports are well below −15 dB, even for TM polarization input. The TM_0-TE_0 polarization conversion loss is lower than 0.73 dB in the wavelength range from 1470 nm to 1580 nm, and the loss that measured at the thru-port for TE_0-TE_0 is lower than 0.7 dB. The crosstalk for TM and TE input are lower than −14.7/−12.1 dB, respectively. The experimental results accords with the theoretical predictions shown in Fig. 3. The crosstalk test results are not as low as expected, which is attributed to the low polarization extinction ratio (around 16 dB) of the laser used in the testing.

4. Design of WDM Receiver

The definition for a high performance integrated receiver includes low loss, low crosstalk, and polarization insensitivity. Polarization insensitive waveguide is a candidate in order to reduce the polarization dependence of a WDM system, while this solution needs specific designed structures, for instance, to make the cross section of the waveguide vertically and horizontally symmetric, which is often not compatible to integration with other devices based on planar CMOS process.

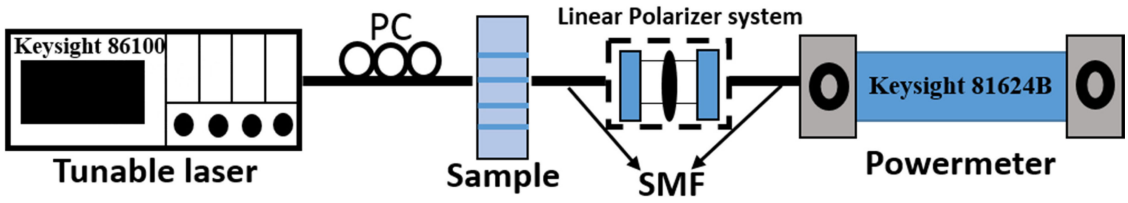

Fig. 4. Experimental setup for on-chip PSR. The test system includes a tunable laser, a polarization controller (for adjusting the polarization state of incident light), a linear polarizer system (to adjust the polarization of the output light), and a power-meter.

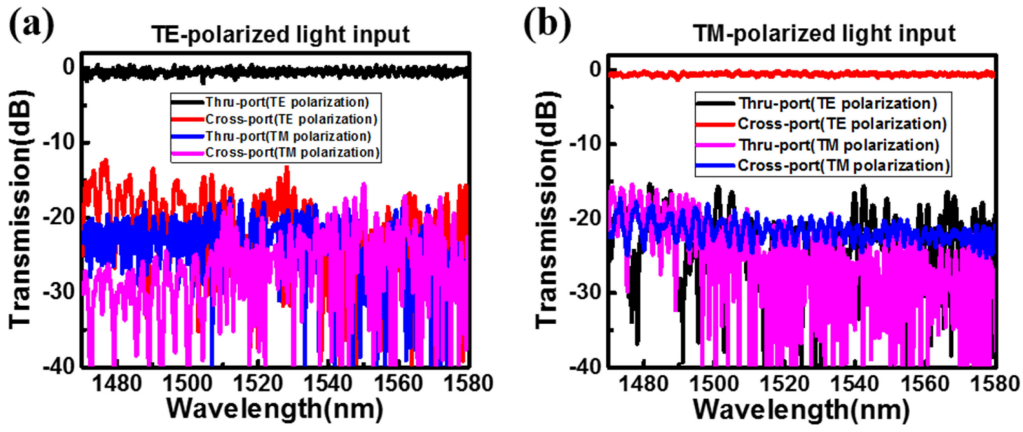

Fig. 5. Testing results at cross and thru ports of (a) TE-polarization light input (b) TM-polarization light input. The measured TE/TM polarization conversion loss is lower than 0.7 dB/0.73 dB with cross talk lower than −12.1 dB/−14.7 dB in the wavelength range from 1470 nm to 1580 nm. All the results are normalized by a reference straight waveguide.

Specifically designed structures [23], [24] can also overcome the polarization-sensitive issue, but this will inevitably leads to performance degradation, as well as complicated fabrication process. In this paper, we use the polarization diversity scheme on the basis of the PSR we proposed to construct the WDM receiver.

Some works are demonstrated to implement the on-chip WDM functionalities, such as etched diffraction gratings (EDGs) [25], [26] AWGs [27], [28], micro-ring resonators (MRRs) [29], [30], and Mach-Zehnder interferometers (MZI) [31], [32]. AWG is widely used in planar integrated optics for its high integration and low cost [33]. A low-loss and low-crosstalk AWG is designed with a channel spacing of 3.2 nm in this work. To reduce the modes mismatch between arrayed waveguides and FPR region, a bi-level taper with its width linearly tapered from 0.45 μm to 2.5 μm is used at the interface which works as a mode converter. The width of the arrayed waveguides is designed to be 1 μm to further reduce phase noises and sensitivity to fabrication errors. Arrayed waveguides with a width of 450 nm are used at bends in order to maintain a small bending radius of 5 μm [34]. At the end, germanium PDs are integrated in each channel to convert the demultiplexed optical signal into electrical signal.

The layout of the integrated WDM receiver is illustrated in Fig. 6(a). An 8-channel monolithically integrated WDM receiver is fabricated on a SOI wafer, which is constructed by a PSR, two 1 $\times$ 8 silicon AWG demultiplexers and a germanium PD for each channel. The TM_0 mode signals will convert to TE_0 mode and then enter to the input port of upper AWG demultiplexer, while the TE_0 mode signals will directly enter the bottom AWG demultiplexer. The upper and bottom AWGs demultiplexer are identical. At last, the de-multiplexed optical signals of the two polarizations for

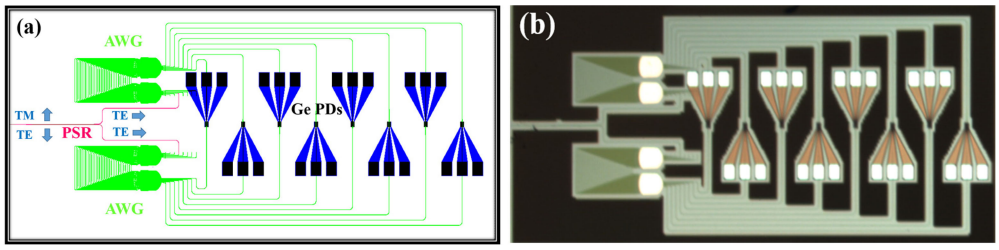

Fig. 6. (a) Layout of the WDM receiver chip. The receiver contains a PSR, two identical 1 × 8 silicon AWG and eight germanium PDs. (b) Microscope image of the integrated WDM receiver.

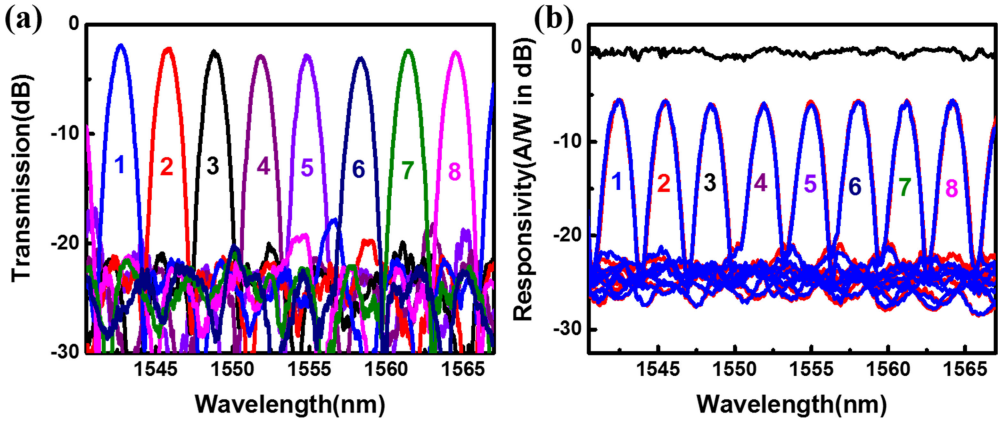

Fig. 7. (a) The measured spectra of the fabricated standalone AWG (b) The measured spectra of WDM receiver at TE (red) polarization, TM (blue) polarization and PDL (black). The fabricated AWG exhibits the maximum insertion loss of 2.88 dB and crosstalk of −18 dB.The test results of WDM receiver shows a polarization dependent loss (PDL) between 1.25 and 2.01 dB and crosstalk of −15 dB.

the same wavelength are sent to the same germanium photodetectors from opposite directions. To reduce the influence of phase differences between two arms, the optical path of two arms after the PSR were identical. Our calculation shows that the time difference is so small even less than 1 ps that it can be ignored.

5. Experimental Results of WDM Receiver

Fig. 7(a) shows the measured spectra of a standalone AWG which has same design with the device used in the WDM receiver. The separate device is tested with the TE polarization input, indicating the maximum insertion loss less than 2.88 dB and crosstalk less than −18 dB. The microscope image of the integrated WDM receiver is demonstrated in Fig. 6(b).The light output from the tunable laser enters the WDM receiver after a polarization controller. The I-V characteristics of the receiver is tested under TE and TM polarization state, respectively. The testing results of the integrated WDM receiver is depicted in Fig. 7(b). Responsivity with TE (red) and TM (blue) polarization state are tested from 1540 nm to 1567 nm. A polarization-dependent loss (PDL) [3], [35] between 1.21 dB and 1.75 dB is shown by the top black line. The calculation method of the PDL refers to formula 1. The PDL contains fabrication errors between the upper and bottom AWG and test errors. The

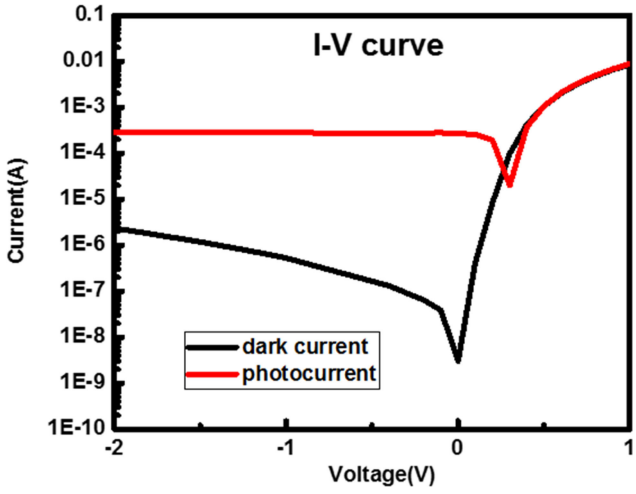

Fig. 8. I-V curves of WDM receiver (red: dark current, black: photocurrent). At -2 V bias, the dark current is about -1.7 μA and photocurrent is about 280 μA.

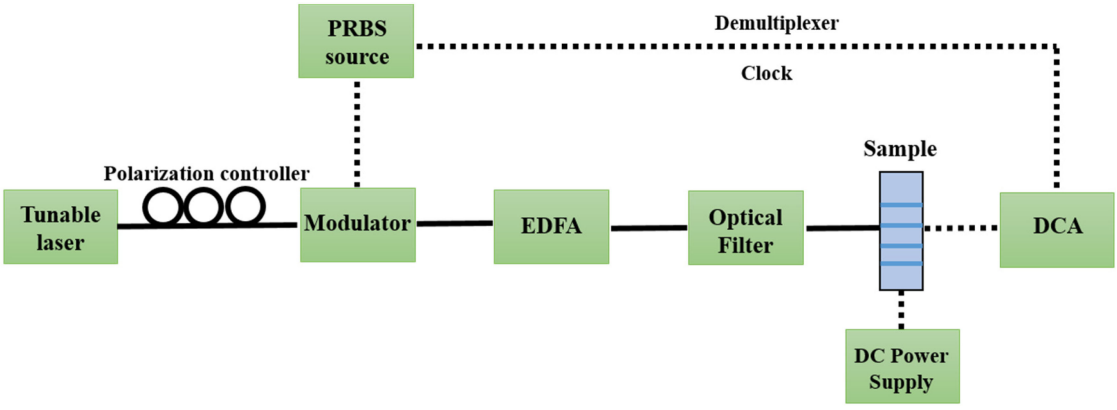

Fig. 9. Exprimental setup for testing eye diagram of WDM receiver.

crosstalk is lower than -15 dB as shown in Fig. 7(b).

$$\text{PDL} = 10 * \log \frac{responsivity\ of\ TE}{responsivity\ of\ TM} \quad \text{(formula 1)}$$

$$\text{responsivity of (TE/TM)} = \frac{photocurrent\ of\ TE/TM}{incident\ light\ power - coupling\ loss} \quad \text{(formula 2)}$$

The dependence of photocurrent and dark current with the voltage of the WDM receiver at room temperature is shown in Fig. 8. The input wavelength is set to 1561.2 nm in the photocurrent test. A photocurrent of 280 μA is generated at -2 V for TE polarization, corresponding to the responsivity of 0.34 A/W (insertion loss of PSR(0.7 dB) and AWG(2.88 dB) included). The calculation method of the responsivity refers to formula 2. The dark current is about -1.7 μA at -2 V.

Eye diagrams are tested with the system shown in Fig. 9. Light output from a tunable laser is first modulated with a commercial $LiNbO_3$ modulator. After that, an EDFA is added to amplify the optical signals. The introduced spontaneous emission noise from the EDFA is filtered out with an optical narrowband filter. Finally, the optical signal is picked up by the sample chip and converted into electrical domain. A polarization controller is also added in the light path to verify the polarization

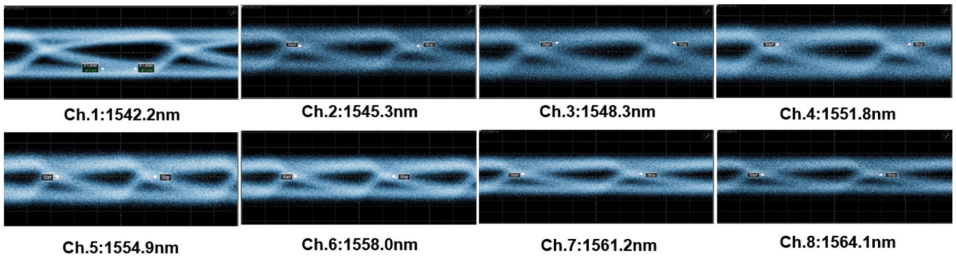

Fig. 10. The measured 10 Gbps electrical eye diagrams of integrated WDM receiver. The Eye diagrams of eight demultiplexed channels are measured with 231^{-1} pseudorandom binary sequence (PRBS) signal under the reverse bias of 2 V with random polarization state.

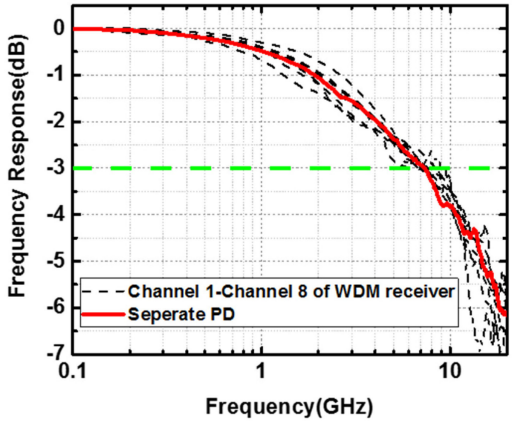

Fig. 11. The measured 3 dB OE bandwidth of WDM receiver of random polarization state and standalone PD of TE polarization state under the reverse bias of 2 V.

TABLE 2

Comparison of Various WDM Receiver.

Year	Author	Components	Cross talk(dB)	PDL(dB)	Number of channels	Data rate(Gbps)
2018	Ourwork	Si PSR; Si AWG; Ge PD	-15	1.21-1.75	8	10
2015	Hang Guan[40]	Bi-level Y-junction; Mach-Zehnder Interferometer based demultiplexers; Monitoring diodes; Ge PD	-9	1.2	4	40
2014	Peter De Heyn[38]	2-dimensional grating coupler; Ring resonators; Ge photodiode	-15	0.5	5	20
2013	Long Chen[3]	Silicon PBS; Si_3N_4 PR; Si_3N_4 AWG; Ge PD	-12	1.2-1.8	10	10
2012	Peter De Heyn[41]	Microring; III-V photodiodes	-17	----------	4	10
2012	Hidetaka Nishi[42]	SiOx AWG; Ge PD	-15	----------	16	1.25
2011	Long Chen[43]	Si_3N_4 AWG; Germanium PD	-20	----------	40	40
1998	M. Kohtoku[44]	Polarization insensitive InP-based AWG; A deep-ridge waveguide structure; InGaAsP PD	-30	1	8	

dependence of the device. It is set at a random position with a fixed polarization state. Random hand tuning of the polarization controller is also done during the test for further verifications.

Eye diagrams of the eight demultiplexed channels are measured with $2^{31}-1$ pseudorandom binary sequence (PRBS) signal at 10 Gbps under the reverse bias of 2 V. The wavelength of each channel is shown in Fig. 10. As illustrated in Fig. 11, the 3 dB bandwidth of WDM receiver and standalone Ge PD are both about 7 GHz. The limited bandwidth is attributed to the design of Ge PD, which has a large size and thus a high RC constant. For further optimization, the length and width of Ge active area in PD can be reduced to achieve greater bandwidth. The clearly opened eyes and 7 GHz 3 dB bandwidth test under the random polarization state means the external polarization state has little impact on the WDM receiver when the proposed PSR is integrated.

Compared to the systems with other polarization-insensitive devices [36]–[39], the complexity of the devices structures and fabrication difficulties are remarkably reduced with the introducing of a PSR.

Table 2 shows the summarized results of WDM receivers. Comparing with these results, a high performance polarization-insensitive WDM receiver is demonstrated based on our silicon PSR and AWG in terms of low channel-crosstalk and PDL. The performance of the WDM receiver could be further improved by optimizing the AWGs and germanium PDs for future applications.

6. Conclusions

A broadband PSR comprised of a bi-level taper and a counter-taper coupler is proposed in this paper, and polarization conversion loss as low as 0.7/0.73 dB and cross talk less than −12.1 dB/−14.7 dB for TE and TM polarizations are achieved respectively, covering a broaden wavelength range from 1470 nm to 1580 nm. An integrated 8-channel WDM silicon receiver is demonstrated by combining the PSR with silicon AWGs and Germanium PDs. The receiver shows polarization insensitive property with PDL as low as 1.21 dB by the polarization diversity scheme. The responsivity of WDM receiver is 0.34 A/W and crosstalk is lower than −15 dB. Clear eye opening at 10 Gbps and 3 dB bandwidth better than 7 GHz in all the eight channels are demonstrated.

References

[1] T. Baehr-Jones, T. Pinguet, P. Lo Guo-Qiang, S. Danziger, D. Prather, and M. Hochberg, “Myths and rumours of silicon photonics,” *Nature Photon.*, vol. 6, no. 4, pp. 206–208, Apr. 2012.
[2] T. Tsuchizawa *et al.*, “Microphotonics devices based on silicon microfabrication technology,” *IEEE J. Sel. Topics Quantum Electron.*, vol. 11, no. 1, pp. 232–240, Jan./Feb. 2005.
[3] L. Chen, “Silicon photonic integrated circuits for WDM technology and optical switch,” in *Proc. Opt. Fiber Commun. Conf. Expo. Nat. Fiber Opt. Eng. Conf.*, Jan. 2013, Paper OW1C.
[4] S. J. Park, C. H. Lee, K. T. Jeong, H. J. Park, J. G. Ahn, and K. H. Song, “Fiber-to-the-home services based on wavelength-division-multiplexing passive optical network,” *J. Lightw. Technol.*, vol. 22, no. 11, pp. 2582–2591, Nov. 2004.
[5] D. Feng *et al.*, “Terabit/s single chip WDM receiver on the SOI platform,” in *Proc. 8th IEEE Int. Conf. Group IV Photon.*, 2011, pp. 320–322.
[6] H. Fukuda, K. Yamada, T. Tsuchizawa, T. Watanabe, H. Shinojima, and S.-I. Itabashi, “Silicon photonic circuit with polarization diversity,” *Opt. Exp.*, vol. 16, no. 7, pp. 4872–4880, 2008.
[7] P. Dong, Y.-K. Chen, G.-H. Duan, and D. T. Neilson, “Silicon photonic devices and integrated circuits,” *Nanophotonics*, vol. 3, no. 4/5, pp. 215–228, 2014.
[8] L. Chen, C. R. Doerr, and Y.-K. Chen, “Compact polarization rotator on silicon for polarization-diversified circuits,” *Opt. Lett.*, vol. 36, no. 4, pp. 469–471, 2011.
[9] T. Barwicz *et al.*, “Polarization-transparent microphotonic devices in the strong confinement limit,” *Nature Photon.*, vol. 1, no. 1, pp. 57–60, 2007.
[10] Y. Ding, H. Ou, and C. Peucheret, “Wideband polarization splitter and rotator with large fabrication tolerance and simple fabrication process,” *Opt. Lett.*, vol. 38, no. 8, pp. 1227–1229, 2013.
[11] Y. Zhang *et al.*, “Ultra-compact and highly efficient silicon polarization splitter and rotator,” *APL Photon.*, vol. 1, no. 9, 2016, Art. no. 091304.
[12] K. Tan, Y. Huang, G.-Q. Lo, C. Lee, and C. Yu, “Compact highly-efficient polarization splitter and rotator based on 90° bends,” *Opt. Exp.*, vol. 24, no. 13, pp. 14506–14512, 2016.
[13] Y. Xiong, D.-X. Xu, J. H. Schmid, P. Cheben, S. Janz, and N. Y. Winnie, “Fabrication tolerant and broadband polarization splitter and rotator based on a taper-etched directional coupler,” *Opt. Exp.*, vol. 22, no. 14, pp. 17458–17465, 2014.

[14] Y. Ding, L. Liu, C. Peucheret, and H. Ou, "Fabrication tolerant polarization splitter and rotator based on a tapered directional coupler," *Opt. Exp.*, vol. 20, no. 18, pp. 20021–20027, 2012.
[15] W. D. Sacher *et al.*, "Polarization rotator-splitters and controllers in a Si_3N_4-on-SOI integrated photonics platform," *Opt. Exp.*, vol. 22, no. 9, pp. 11167–11174, 2014.
[16] Y. Ma *et al.*, "Symmetrical polarization splitter/rotator design and application in a polarization insensitive WDM receiver," *Opt. Exp.*, vol. 23, no. 12, pp. 16052–16062, 2015.
[17] Y. Ding, H. Ou, and C. Peucheret, "Wideband polarization splitter and rotator with large fabrication tolerance and simple fabrication process," *Opt. Lett.*, vol. 38, no. 8, pp. 1227–1229, 2013.
[18] D. Dai, Y. Tang, and J. E. Bowers, "Mode conversion in tapered submicron silicon ridge optical waveguides," *Opt. Exp.*, vol. 20, no. 12, pp. 13425–13439, 2012.
[19] D. Dai and J. E. Bowers, "Novel concept for ultracompact polarization splitter-rotator based on silicon nanowires," *Opt. Exp.*, vol. 19, no. 11, pp. 10940–10949, 2011.
[20] X. Chen *et al.*, "Design of an ultra-broadband and fabrication-tolerant silicon polarization rotator splitter with SiO2 top cladding," *Chin. Opt. Lett.*, vol. 14, no. 8, Aug. 10, 2016.
[21] N. Riesen and J. D. Love, "Tapered velocity mode-selective couplers," *J. Lightw. Technol.*, vol. 31, no. 13, pp. 2163–2169, Jul. 2013.
[22] L. Liu, Y. H. Ding, K. Yvind, and J. M. Hvam, "Silicon-on-insulator polarization splitting and rotating device for polarization diversity circuits," *Opt. Exp.*, vol. 19, no. 13, pp. 12646–12651, Jun. 20, 2011.
[23] T. Lang, J.-J. He, J.-G. Kuang, and S. He, "Birefringence compensated AWG demultiplexer with angled star couplers," *Opt. Exp.*, vol. 15, no. 23, pp. 15022–15028, 2007.
[24] Z. Wang, D. Dai, and S. He, "Polarization-insensitive ultrasmall microring resonator design based on optimized Si sandwich nanowires," *IEEE Photon. Technol. Lett.*, vol. 19, no. 20, pp. 1580–1582, Oct. 2007.
[25] J. Brouckaert, W. Bogaerts, P. Dumon, D. V. Thourhout, and R. Baets, "Planar concave grating demultiplexer fabricated on a nanophotonic silicon-on-insulator platform," *J. Lightw. Technol.*, vol. 25, no. 5, pp. 1269–1275, May 2007.
[26] D. Chowdhury, "Design of low-loss and polarization-insensitive reflection grating-based planar demultiplexers," *IEEE J. Sel. Topics Quantum Electron.*, vol. 6, no. 2, pp. 233–239, Mar./Apr. 2000.
[27] J. Zou, X. Jiang, X. Xia, T. Lang, and J. J. He, "Ultra-compact birefringence-compensated arrayed waveguide grating triplexer based on silicon-on-insulator," *J. Lightw. Technol.*, vol. 31, no. 12, pp. 1935–1940, Jun. 2013.
[28] T. Ye, Y. Fu, L. Qiao, and T. Chu, "Low-crosstalk Si arrayed waveguide grating with parabolic tapers," *Opt. Exp.*, vol. 22, no. 26, pp. 31899–31906, 2014.
[29] X. Zheng *et al.*, "A tunable 1×4 silicon CMOS photonic wavelength multiplexer/demultiplexer for dense optical interconnects," *Opt. Exp.*, vol. 18, no. 5, pp. 5151–5160, 2010.
[30] F. Xia, M. O'Boyle, L. Sekaric, and Y. Vlasov, "Ultra-compact wavelength division multiplexing devices using silicon photonic wires for on-chip interconnects," in *Proc. Opt. Fiber Commun. Conf. Expo. Nat. Fiber Opt. Eng. Conf.*, Anaheim, CA, USA, 2007, Paper OWG2.
[31] F. Horst, W. M. J. Green, S. Assefa, S. M. Shank, Y. A. Vlasov, and B. J. Offrein, "Cascaded Mach-Zehnder wavelength filters in silicon photonics for low loss and flat pass-band WDM (de-)multiplexing," *Opt. Exp.*, vol. 21, no. 10, pp. 11652–11658, 2013.
[32] S.-H. Jeong, S. Tanaka, T. Akiyama, S. Sekiguchi, Y. Tanaka, and K. Morito, "Flat-topped and low loss silicon-nanowire-type optical MUX/DeMUX employingmulti-stage microring resonator assisted delayed Mach-Zehnder interferometers," *Opt. Exp.*, vol. 20, no. 23, pp. 26000–26011, 2012.
[33] Z. Zhang *et al.*, "Low-crosstalk silicon photonics arrayed waveguide grating," *Chin. Opt. Lett.*, vol. 15, no. 4, 2017, Art. no. 041301.
[34] J. Wang *et al.*, "Low-loss and low-crosstalk 8 x 8 silicon nanowire AWG routers fabricated with CMOS technology," *Opt. Exp.*, vol. 22, no. 8, pp. 9395–9403, Apr. 21, 2014.
[35] L. Chen, C. R. Doerr, and Y.-K. Chen, "Polarization-diversified DWDM receiver on silicon free of polarization-dependent wavelength shift," in *Proc. Opt. Fiber Commun. Conf.*, 2012, Paper OW3G. 7.
[36] D. Feng *et al.*, "Terabit/s single chip WDM receiver on the SOI platform," in *Proc. 8th IEEE Int. Conf. Group IV Photon.*, 2011, Paper FA2.
[37] T. Pinguet, B. Analui, G. Masini, V. Sadagopan, and S. Gloeckner, "40-Gbps monolithically integrated transceivers in CMOS photonics," *Proc. SPIE*, vol. 6898, 2008, Art. no. 689805.
[38] P. De Heyn *et al.*, "Polarization-insensitive 5×20 Gb/s WDM Ge receiver using compact Si ring filters with collective thermal tuning," *Opt. Fiber Commun. Conf.*, 2014, Paper Th4C.5.
[39] C. Doerr, L. Chen, L. Buhl, and Y. Chen, "Eight-channel $SiO_2/Si_3N_4/Si$/Ge CWDM receiver," *IEEE Photon. Technol. Lett.*, vol. 23, no. 17, pp. 1201–1203, Sep. 2011.
[40] H. Guan *et al.*, "Polarization-insensitive 40 Gb/s 4-WDM channels receiver on SOI platform," in *Proc. Opt. Interconnects Conf.*, 2015, pp. 54–55.
[41] P. De Heyn, S. Verstuyft, S. Keyvaninia, A. Trita, and D. Van Thourhout, "Tunable 4-channel ultra-dense WDM de-multiplexer with III–V photodiodes integrated on silicon-on-insulator," in *Proc. Commun. Photon. Conf.*, Nov. 2012 pp. 1–3.
[42] H. Nishi *et al.*, "Monolithic integration of a silica AWG and Ge photodiodes on Si photonic platform for one-chip WDM receiver," *Opt. Exp.*, vol. 20, no. 8, pp. 9312–9321, 2012.
[43] L. Chen, C. R. Doerr, L. Buhl, Y. Baeyens, and R. A. Aroca, "Monolithically integrated 40-wavelength demultiplexer and photodetector array on silicon," *IEEE Photon. Technol. Lett.*, vol. 23, no. 13, pp. 869–871, Jul. 2011.
[44] M. Kohtoku, H. Sanjoh, S. Oku, Y. Kadota, and Y. Yoshikuni, "Polarization independent semiconductor arrayed waveguide gratings using a deep-ridge waveguide structure," *IEICE Trans. Electron.*, vol. 81, no. 8, pp. 1195–1204, 1998.